Journal of Marine Research, 45, 259–291, 1987

Journal of
MARINE RESEARCH

Volume 45, Number 2

Lagrangian properties of eddy fields in the northern North Atlantic as deduced from satellite-tracked buoys

by W. Krauss[1] and C. W. Böning[1]

ABSTRACT

One hundred and thirteen satellite-tracked buoys have been used during their first 5 months after deployment in order to calculate Lagrangian statistics of the eddy field in the northern North Atlantic between Newfoundland and the Canary basin. r.m.s. velocities are isotropic and increase from southeast to northwest. Lagrangian integral time scales, derived both from correlation function and from dispersion, are slightly anisotropic and decrease from the subtropics toward the North Atlantic Current. Time scale is inversely proportional to the r.m.s. velocity of the eddies. Eddy length scale is approximately constant in the North Atlantic. Dispersion is in good agreement with Taylor's hypothesis, following a t^2-law during the first day after release and a linear increase with time during days 10 to 60.

Eddy diffusivity increases from 30N to 50N by a factor of about 4 and is linearly dependent on the r.m.s. velocity. The energy containing frequency band of the eddies shifts toward higher frequencies in the northern part of the Atlantic. Beyond the cut-off frequency of the eddies the spectral slope follows a -2 or -3 power law.

1. Introduction

During the years 1981 to 1984 more than 100 satellite-tracked drifting buoys were deployed in the northern North Atlantic by the Institut für Meereskunde, Kiel. All of them were of the HERMES type, drogued with a window-shade sail. The buoys were used to analyze the large-scale mean circulation (Krauss, 1986) and the eddy field (Krauss and Käse, 1984).

Most deployments took place during mesoscale hydrographic surveys of box-like

1. Institut für Meereskunde an der Universität Kiel, Dusternbrooker Weg 20, D-2300 Kiel 1, West Germany.

areas which had a typical size of 5° latitude by 5° longitude. In all cases the dynamic topography of these areas was dominated by cyclonic and anticyclonic eddies of an approximate scale of 100 to 200 km. Buoys, released during the surveys, followed relatively close the height contours (Krauss and Käse, 1984, Fig. 16; Krauss and Meincke, 1982, Fig. 3). During their initial time of drift these buoys were good indicators of the observed mesoscale eddy field. After about 2 weeks of drift they indicated that the eddies changed in shape and size.

The use of free-drifting buoys for measuring current systems has become increasingly common during the last years. Trajectories give direct insight into the particle drift and allow us to obtain an easy description of both large-scale flows and eddy fields. Examples with respect to large-scale patterns are the near-surface circulation of the subtropical gyre of the North Pacific (McNally *et al.*, 1983) and the separation of the North Atlantic Current from the subtropical gyre of the North Atlantic (Krauss, 1986).

In numerous cases satellite-tracked buoys have been used to study the kinematics of eddies and rings. Richardson (1983) was the first who used all available tracks in the western North Atlantic to construct maps of eddy kinetic energy. These maps have been later complemented by similar ones for the northeastern part of the North Atlantic and show the Gulf Stream and the North Atlantic Current as a continuous band of high eddy kinetic energy (Krauss and Käse, 1984).

Eddy kinetic energy, however, is a rough measure of the intensity of the eddy field in the ocean. With increasing number of buoys available, more precise quantities can be derived. Using a set of sixteen buoys Colin de Verdiere (1983) made the first attempt to compute Lagrangian statistics from surface drifters in a local area (47N, 11W) of the eastern North Atlantic. Similar calculations have been carried out by Davis (1985) for the waters on the continental shelf off northern California, using a total of 164 surface drifters. The present data set offers the possibility to derive Lagrangian statistics for a wide area of the North Atlantic and to arrive at a better understanding of the eddy field in the ocean.

Our present knowledge of that eddy field is incomplete. Eddies exist nearly everywhere in the ocean (Robinson, 1983), but their role in the dynamics is barely understood (Holland *et al.*, 1983). Observations show that the ocean is strongly turbulent, however, only very few quantitative measures of this turbulence are available at present. These measures are required to help develop realistic models of the ocean circulation (Schmitz and Holland, 1982).

Lagrangian measurements address directly those features of the velocity field which are important for describing the transport of passive tracers. Recent experiments (Cox, 1985) on the distribution of potential vorticity demonstrate that dispersion by eddies can modify the large-scale distribution of passive scalars considerably. Lagrangian statistics provide the most direct description of property transport (Davis, 1983).

Furthermore, Lagrangian statistics are the most sensitive statistical method to test

the validity of eddy resolving models. In order to properly choose the parameters used in these models the Lagrangian statistics of the model output (Haidvogel, 1984) should be comparable to the Lagrangian statistics of drifting buoys or floats.

The present study is an attempt to derive quantitative results for a number of areas in the northern North Atlantic. After a short summary of the basic statistical quantities we describe the data set, compute elementary statistics and test their stability with respect to the averaging intervals. We then try to determine the Lagrangian time scale, which plays a fundamental role in the particle dispersion. This is followed by a test of Taylor's theorem on single particle dispersion and Lagrangian diffusivity. We finally present Lagrangian spectra of the floats. The area under consideration is the North Atlantic between Newfoundland (Flemish Cap) and the Canary basin.

Like any other floating device drogued surface buoys are only quasi-Lagrangian particles. Similar to SOFAR floats (Riser, 1982) they drift along horizontal surfaces, whereas water particles may follow layers of constant density. Additionally, buoy tracks may represent an integrated effect of currents and wind influences. The hydrographic surveys mentioned above suggest, however, that the trajectories are not severely contaminated by windage, as long as the buoys were drogued by a sail. To guarantee this in our statistical calculations, we limit our trajectories to 5 months after deployment.

2. Lagrangian statistics

Given a set of drifting buoys, the Lagrangian description of motion is in terms of the buoy position $\mathbf{r}$ as function of time,

$$\mathbf{r}_p = \mathbf{r}_p(t, \mathbf{r}_{op}) \qquad p = 1, 2, , \ldots \tag{1}$$

where $\mathbf{r}_{op}$ is the position of deployment of buoy number p (the buoy identification). We limit the time series (the range over which the buoys drift) in such a way (5 months) that we can assume homogeneity. In Section 3 it will be shown that the eddy velocity field is isotropic. Thus, in the following we shall apply the theory of homogeneous isotropic turbulence.

Buoys in eddy fields are scattered over large areas (Krauss, 1986) and, consequently, are exposed to the large-scale inhomogeneous mean current field. Furthermore, eddy kinetic energy decreases from the Gulf Stream extension area toward the east. Therefore, we cannot assume stationarity for the random function $\mathbf{r}(t)$ given by the realizations $\mathbf{r}_p(t)$. However, for a limited time range, the instationarity of the random process $\mathbf{r}$ can be approximated by a linear function, which implies, that the increments of $\mathbf{r}$ form a stationary process. In other words, the velocities $\mathbf{v}$, computed for 3-hourly intervals according to $\mathbf{v} = [\mathbf{r}(t + 3h) - \mathbf{r}(t)]/3h$, can be treated as a stationary random process (Panchev, 1971).

Let u, v be east and north components of the velocities v. We first compute the mean velocity $\bar{u}$, $\bar{v}$, and the standard deviation $\sqrt{\overline{u'^2}}$, $\sqrt{\overline{v'^2}}$, due to the eddy field. The determination of a (weak) mean velocity in a vigorous eddy field requires long time series. This is in conflict with our limitation of the series by 5 months in order to guarantee homogeneity. Stable mean values can only be obtained by a large number of drifters. They will be presented as

$$\bar{u} \pm \frac{2\sqrt{\overline{u'^2}}}{\sqrt{N_m}}, \tag{2}$$

where $\bar{u}$ is the mean value of u averaged over time and all realizations and $\sqrt{\overline{u'^2}}$ is the corresponding standard deviation. If we have N^* observations and T is the Lagrangian integral time scale (to be defined later) than we have $N_m = N^*/T$ statistically independent data.

The second term in (2) gives the error of the mean value (95% confidence interval according to Student-t-test; see also Riser and Rossby, 1983; Flierl and McWilliams, 1977). Accordingly, the error of the standard deviation is described by the 95% confidence interval, assuming a Gaussian distribution of the eddy scale motion. The r.m.s. velocities are given as

$$\sqrt{\overline{u'^2}}\,(1 \pm 1.96 / \sqrt{2N_m}). \tag{3}$$

The Lagrangian integral time scale T is defined by

$$T = \int_0^\infty R(\tau)\, d\tau,\ R(\tau) = \frac{1}{\overline{u'^2}\, T_{\max}} \int_0^{T_{\max}} u'(t)u'(t+\tau)\, dt \tag{4}$$

where R is the normalized autocorrelation function.

In case of a pure random walk the Lagrangian integral time scale is a measure of the time scale during which $u'(t)$ correlates with itself. After time T the fluctuations are statistically independent.

Two problems are encountered in determining T, which have their origin in the finite length of the time series, $T_{\max}$:

(i) correlation functions often consist of a decaying and an oscillatory component. As the integration in (4) cannot be extended to infinity the oscillatory component falsifies T. Most often the negative lobes dominate the results, giving too short integral time scales.

(ii) sometimes correlation functions do not approach zero, which seems to be due to a bad separation of the mean current from the fluctuations. In this case, T appears larger.

To overcome the difficulties described under (i) and (ii), at least partially, we use the

structure function in order to determine T. The structure function

$$D(\tau) = \overline{[u\,(t+\tau) - u(t)]^2} \tag{5}$$

is related to the (non-normalized) correlation function $B(\tau)$ according to

$$D(\tau) = 2[B(o) - B(\tau)] = 2[\overline{u'^2} - B(\tau)],\ B(\tau) = \overline{u'^2}\,R(\tau). \tag{6}$$

In all our examples the correlation function is determined from the structure function $D(\tau)$ as defined by (6), because the calculation of $D(\tau)$ is less sensitive to large random deviations (Panchev, 1971) than the direct calculation of R. This holds especially if the mean value is uncertain.

Having determined the Lagrangian time scale we compute single particle dispersion, i.e. the dispersion of a particle from its origin. According to Taylor (1921), the particle dispersion is related to the correlation function as

$$\overline{x'^2(t)} = 2\,\overline{u'^2}\int_0^t (t-\tau)R(\tau)d\tau = 4\int_0^\infty E(\omega)\,\frac{\sin^2(\omega t/2)}{\omega^2}\,d\omega \tag{7}$$

where $x'(t)$ is the displacement of the particle due to u' and $E(\omega)$ is the energy spectrum of u'. Taylor's result in form of (7) is due to Kampe de Feriet (1939). Eq. (7) approaches two limits independent from the special form of $R(\tau)$, just resulting from $R = 1$ at $\tau = 0$ and $R \to 0$ for τ very large:

$$\text{if } t \to 0, \text{ i.e. } t < T \text{ then } \overline{x'^2} = \overline{u'^2}t^2 \text{ (the initial dispersion)} \tag{8}$$

$$\text{if } t \gg T \text{ then } \overline{x'^2} = 2\overline{u'^2}Tt \text{ (the random walk regime).} \tag{9}$$

As diffusion for large time scales is proportional to time, the Lagrangian diffusivity $K_{ii} = \frac{1}{2}\,d\overline{x'^2}/dt$ is given by

$$K_{ii} = \overline{u_i'^2}\int_0^t R(\tau)d\tau = \overline{u_i'^2}\,T. \tag{10}$$

Relation (9), if satisfied, can be used to determine the Lagrangian integral scale from $\overline{x'^2}$ and $\overline{u'^2}$, independently from (4).

Another important quantity is the Lagrangian length scale, i.e. the distance over which the particle remembers its path during a random walk. It is given by

$$L = \sqrt{\overline{u'^2}}\,T. \tag{11}$$

3. The data set

A total of 113 buoys, deployed in the North Atlantic during 1981-1984, is used for this analysis. They were drogued in 100 m depth. A window-shade drogue element was used in all cases. The reason for having the drogue at 100 m was to measure the geostrophic flow below the Ekman layer.

In Figure 1 we display the used trajectories which form the data base. Their

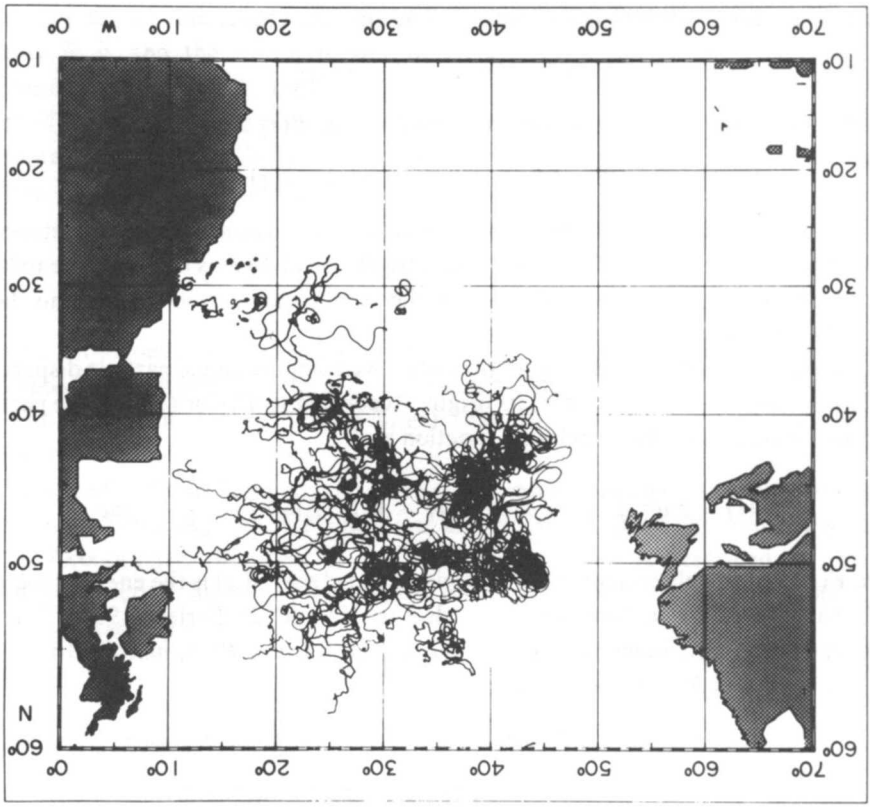

Figure 1. Buoy trajectories of 113 satellite-tracked buoys based on daily averages. The first 5 months after deployment are shown.

maximum length is 5 months. One reason for the limitation is to avoid undrogued buoys. A further reason for this limitation of the series is the assumption of homogeneous and stationary turbulence, which holds only for areas of several eddy scales.

In order to meet the above condition, drifters have been grouped to 8 ensembles according to the center-of-mass during their 5-month drift after deployment. In Figure 2 the areas of these groups are shown in form of the mean position of each ensemble (+) and its standard deviation with respect to ϕ and λ (rectangle). In Table 1 we list these data together with the number of buoy days available for each ensemble and the number of buoys from which they are obtained. The data used to compute the Lagrangian statistics are time series of position and velocity with a 3-hour interval, averaged over one day in order to remove the high frequency part of the fluctuations. With the exception of the northernmost ensembles 7 and 8, more than 1000 buoy days are available in each group. Ensemble 8 is the least reliable.

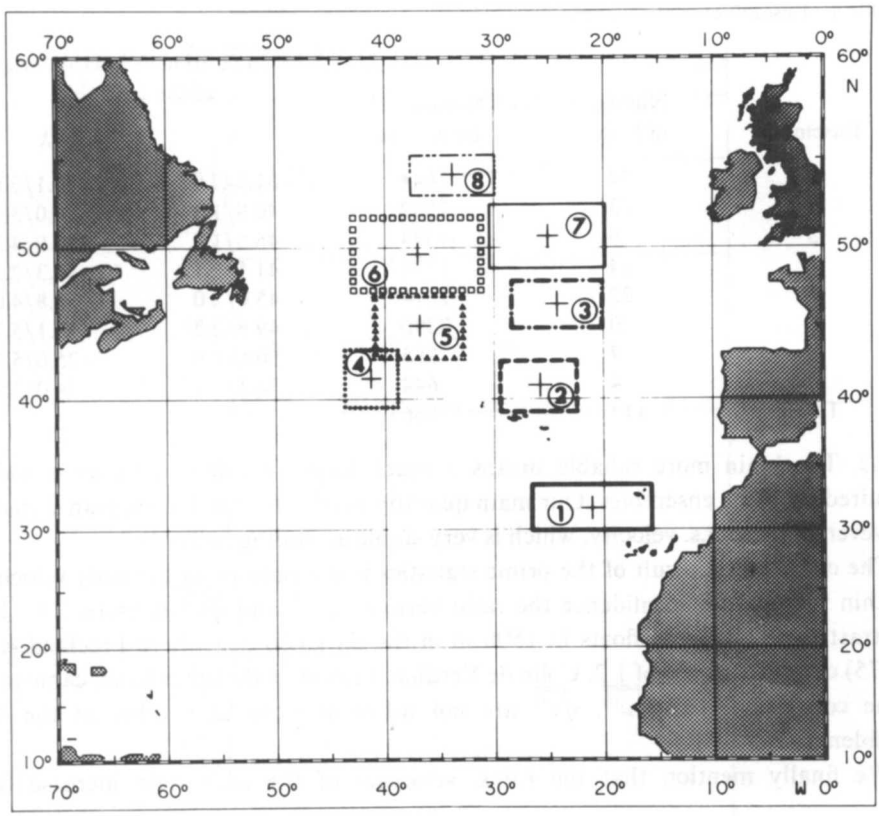

Figure 2. Center-of-mass of ensembles 1 to 8 (the cross marks the mean position) and standard deviation with respect to ϕ and λ (rectangle).

4. Prime statistics

The results of prime statistics according to Eqs. (2) and (3) are summarized in Table 2. Mean value and standard deviation have been obtained by averaging over time and ensemble. The r.m.s. velocities of the eddy field are significant for all ensembles, on the average they exceed the mean values considerably.

The mean values are less reliable. Those which are significantly different from zero have been underlined in Table 2. The large uncertainty in the mean value results from the short length of the records (5 months at the maximum) and the limited number of buoys per ensemble. To elucidate the dependency of the computed mean values on the number of data points (days) used for averaging, Figure 3 depicts $\bar{u}$, $\bar{v}$ and $\sqrt{\overline{u'^2}}$, $\sqrt{\overline{v'^2}}$ as function of the averaging interval for two ensembles. In general about 1000 buoy days are required to stabilize the mean value at its proper level, and even 2000 (more than 5 years) to obtain an accurate value. As the mean values between 30N and 50N vary between about 0 and 8 cm s^{-1}, homogeneity can be assumed only for rather small

Table 1. Ensembles of drift buoys.

Ensemble	Number of buoys	Number of buoy days	Mean position/standard deviation of the ensemble ϕ	λ
1	14	1644	31.8/2.0	−21.1/5.6
2	23	2582	40.8/1.8	−26.0/3.6
3	9	1378	46.5/1.7	−24.0/4.2
4	14	1329	41.5/2.1	−41.3/2.3
5	22	2514	45.0/2.0	−36.8/4.0
6	20	2290	49.6/2.2	−37.1/5.7
7	7	885	50.6/1.9	−25.0/5.3
8	4	644	54.1/1.1	−34.0/3.9
Total	113	13266		

areas. To obtain more reliable means a much larger number of buoys would be required for some ensembles. Our main quantity needed for the Lagrangian statistics, however, is the r.m.s. velocity, which is very stable according to Table 2.

The outstanding result of the prime statistics is the isotropy of the eddy velocities. Within the limits of confidence the ratio between $\sqrt{\overline{u'^2}}$ and $\sqrt{\overline{v'^2}}$ is unity. This is in contrast to results from floats in 1500 m in the Sargasso Sea where Freeland *et al.* (1975) obtained a ratio of 1.2. Colin de Verdiere (1983) on the other hand, came to the same conclusion that $\sqrt{\overline{u'^2}}$, $\sqrt{\overline{v'^2}}$ are not different from each other at the 95% confidence level.

We finally mention that the r.m.s. velocities of the eddy field increase from

Table 2. Primary statistics.

Ensemble	Number of buoy days N*	Mean velocities $\overline{u}$ / $\overline{v}$	standard deviation u_{rms} / v_{rms}
1	1644	−0.4 ± 0.9	8.2 ± 0.6
		−1.5 ± 1.0	8.2 ± 0.7
2	2582	3.0 ± 1.3	10.8 ± 0.9
		−1.0 ± 1.0	10.7 ± 0.7
3	1378	6.1 ± 2.1	14.0 ± 1.3
		0.9 ± 1.8	14.1 ± 1.0
4	1329	2.9 ± 1.9	20.7 ± 1.4
		−2.8 ± 2.0	21.3 ± 1.2
5	2514	6.9 ± 1.5	23.2 ± 1.1
		−0.3 ± 1.6	23.8 ± 1.2
6	2290	8.3 ± 1.5	24.6 ± 1.0
		2.6 ± 1.5	25.8 ± 1.1
7	885	7.9 ± 2.7	21.5 ± 1.8
		1.4 ± 2.5	19.5 ± 1.3
8	644	3.5 ± 4.1	17.3 ± 1.9
		1.3 ± 3.0	16.7 ± 1.6

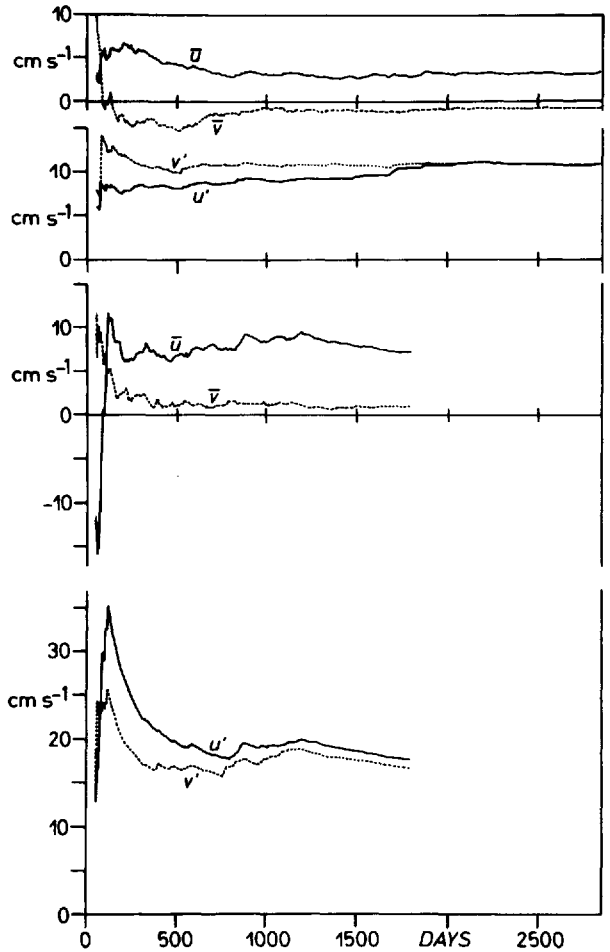

Figure 3. Mean velocities $\bar{u}$, $\bar{v}$ and r.m.s. velocities $\sqrt{\overline{u'^2}}$, $\sqrt{\overline{v'^2}}$ as function of increasing averaging interval for 2 ensembles (to simplify the fig., u' stands for $\sqrt{\overline{u'^2}}$).

southeast (Canary Islands) toward northwest, where they reach maximum values in the North Atlantic Current east of Flemish Cap. Beyond the Subarctic front (ensemble 8) the intensity gradually decreases.

5. Lagrangian scales as derived from autocorrelation functions

In Figure 4 we display the structure functions $\sqrt{D}$ according to Eq. (5). In the ideal case the structure function should increase rapidly to the saturation level and then should remain constant. In all real cases the data base becomes small for large lags and, therefore, the structure function varies randomly with increasing τ. To avoid influences from these fluctuations at large lags we have chosen the saturation level as

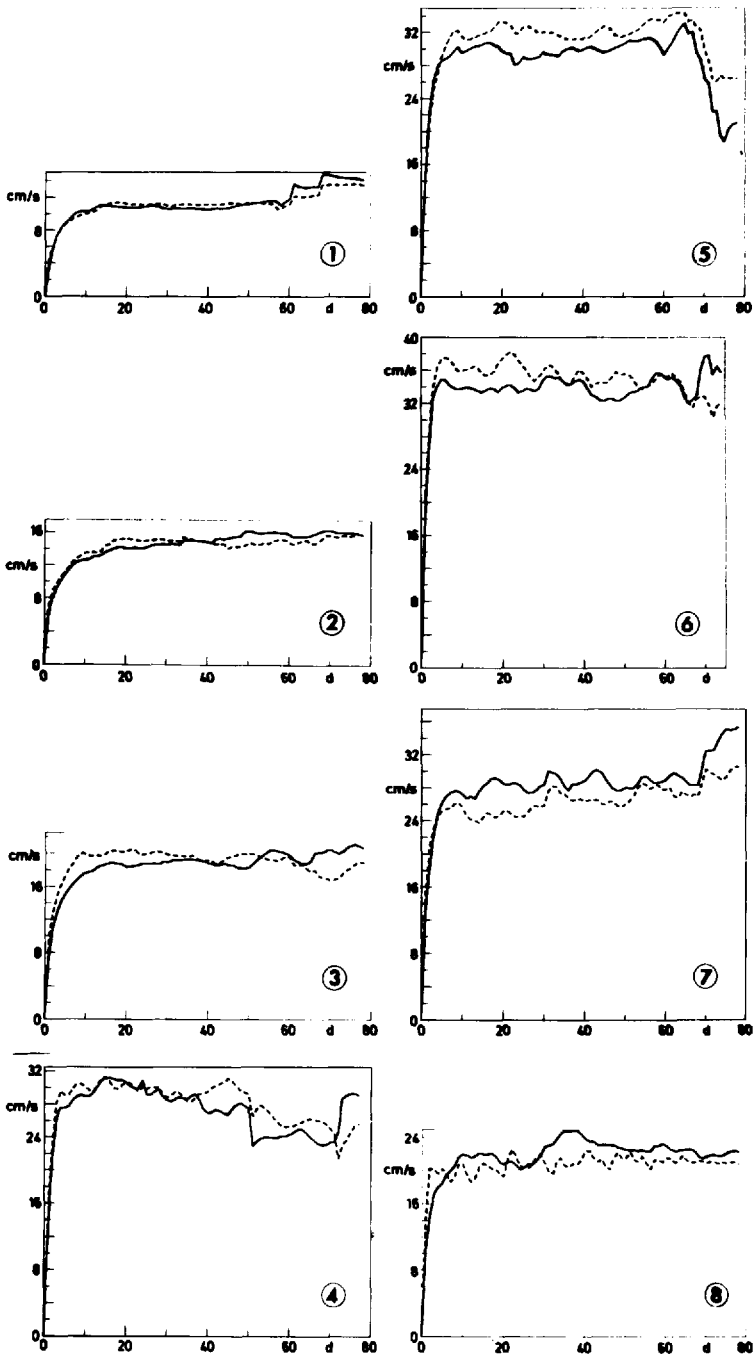

Figure 4. Structure function D (km) as a function of time (days) for ensembles 1 to 8 (full line u', broken line v').

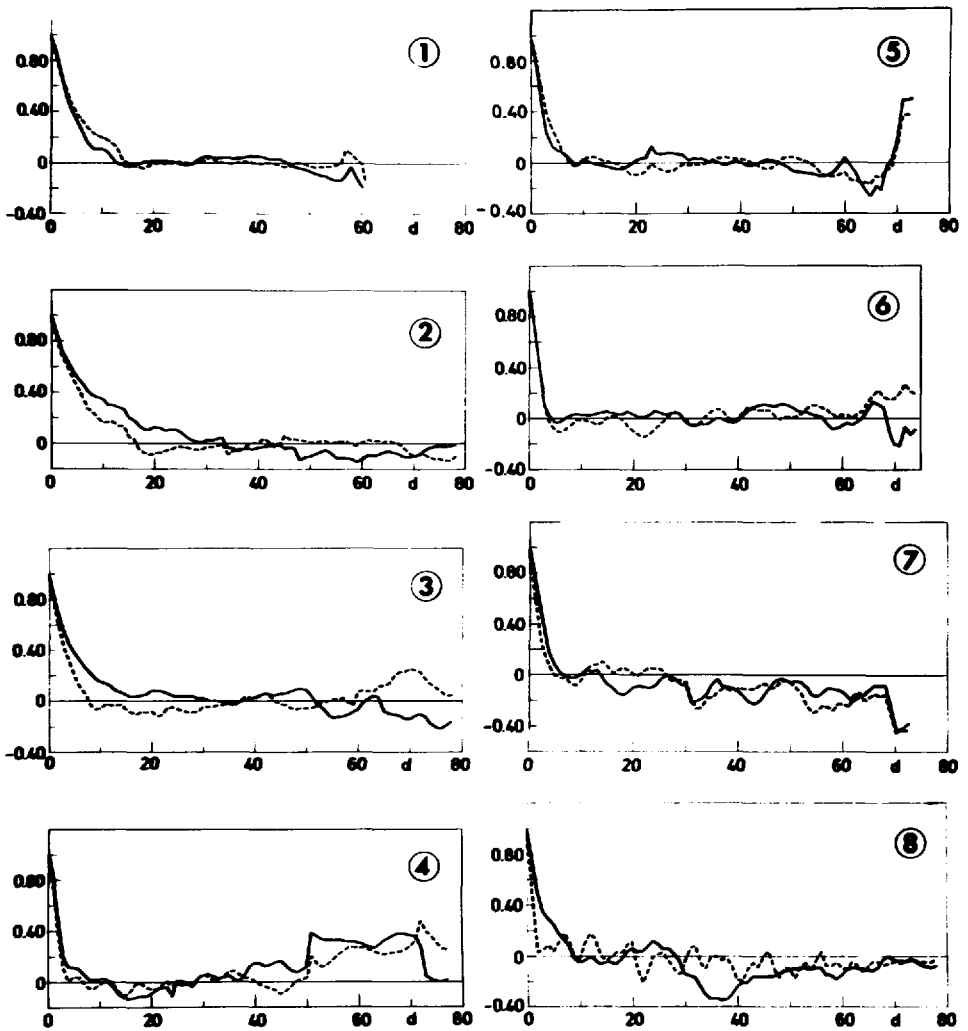

Figure 5. Autocorrelation function for u' (full line) and v' (dashed line) as derived from the structure function for ensembles 1 to 8.

the average of the structure function between 20 and 60 days. In the case of ensemble 4 the range from 15–50 days has been selected. The autocorrelation functions were computed from the structure function as outlined in Section 2 and are depicted in Figure 5.

In comparing Figures 4 and 5 one has to bear in mind that the structure function appears smoother also due to plotting $\sqrt{D}$ instead of D. As typical for real data, most of the autocorrelation functions do not approach zero or show a systematic trend, which

Table 3. Lagrangian time scales (days) and length scales (km) as derived from the autocorrelation functions.

	Time scale		Length scale	
Ensembles	Zonal	Meridional	Zonal	Meridional
1	4.5	5.6	32	40
2	8.6	5.9	80	53
3	6.0	3.4	72	41
4	3.0	2.3	53	42
5	2.8	3.2	56	66
6	2.1	2.1	45	47
7	3.2	2.2	59	37
8	4.0	2.9	60	42
Mean	4.3	3.4	58	46

strongly influences the integral time scale. We, therefore, adopt the usual praxis to integrate from zero to the time of the first zero crossing, which corresponds to integrate the structure function from zero to the saturation level, given by $D = 2\ \overline{u'^2}$. This procedure is not satisfactory but seems to be more appropriate to correlation functions which vary arbitrarily for higher lags. We thus discard the values beyond the first zero crossing and consider them not to be confident. Due to the uncertainty of the mean value the error in T may be as large as 20–30%. The results are listed in Table 3, columns 2 and 3. The values can be considered as upper bounds to the true time scale because we neglect negative lobes also in cases when they are real.

On the average the zonal time scale (4.3 days) is longer than the meridional one (3.4 days). One exception is ensemble 1 which shows many descrepancies compared to the other ensembles. Ensemble 1 belongs to the subtropical gyre whereas all other ensembles are typical for the North Atlantic Current and the westwind drift. Different dynamical processes may, therefore, determine the short zonal time scales of ensemble 1. For ensembles 2 to 7 we note a decrease of the integral time scale from southeast to northwest. This difference in time scale is also obvious from inspection of Figure 5. Anisotropy between zonal and meridional scales is present in nearly all cases. Again comparing the results with those of Freeland *et al.* (1975) and Colin de Verdiere (1983), who observed time scales of 10 days and about a week, respectively, we find these values comparable but somewhat larger than ours at subtropical latitudes. However, the results of these authors are not representative for the northern part of the Atlantic.

Ensemble 8, the only group beyond the Subarctic front, yields a longer time scale compared to others. This ensemble, however, is the least reliable. Another difference between the southern and the northern ensembles is the oscillatory component in the autocorrelation function. These oscillation of 6–8 days are well pronounced in the meridional autocorrelation function of ensemble 6 to 8 which are in the North Atlantic

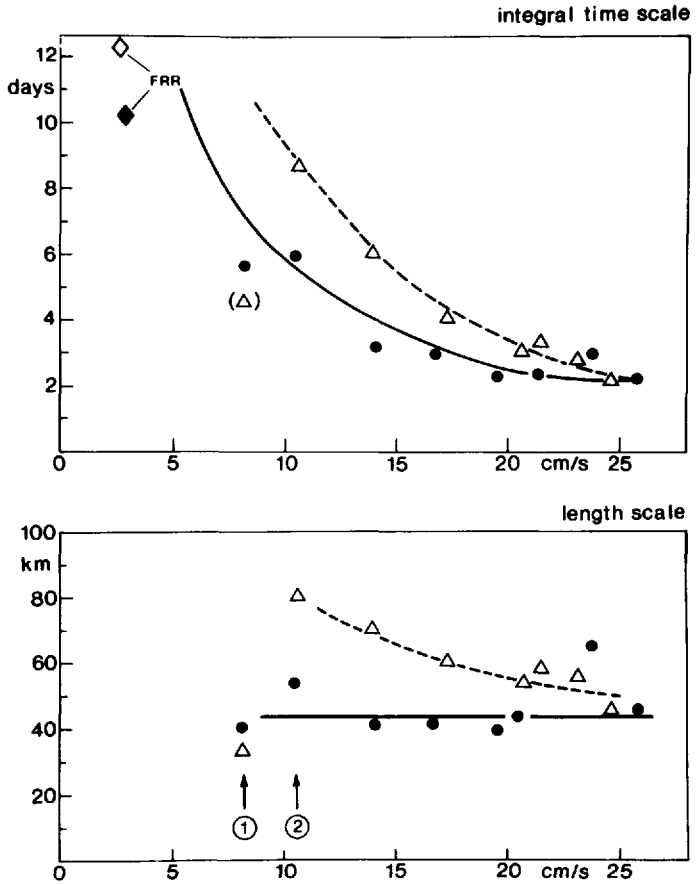

Figure 6. Integral time scale and length scale as function of r.m.s. velocity (FRR = Freeland *et al.*, 1975). The arrows mark ensembles 1 and 2. Triangles refer to zonal, dots to meridional scales).

Current. They do not appear farther south. A possible candidate for these oscillations is barotropic Rossby waves due to the storms passing over these northerly regions.

Closely related to the Lagrangian time scale is the Lagrangian length scale, which is defined by Eq. (11) and is also listed in Table 3. As the r.m.s. velocities are isotropic, L is anisotropic like T. In Figure 6 we depict both T and L as function of the r.m.s. velocity. Obviously, the Lagrangian time scale decreases with increasing eddy velocity. This decrease is more intensive for the zonal component than the meridional one. An exception is again given by the zonal time scale of ensemble 1. The data of Freeland *et al.* (1975) fit well into the picture.

The inverse proportionality between T and $\sqrt{\overline{u'^2}}$ is to be anticipated from scaling arguments if the eddies have nearly constant horizontal scale (McWilliams *et al.*,

1983). The relation between T and $\sqrt{\overline{u'^2}}$ is:

$$T_{11} = -2.7 + 121.2/\sqrt{\overline{u'^2}}\ T_{22} = -0.4 + 61.0/\sqrt{\overline{v'^2}}. \tag{12}$$

The correlation coefficient is .99 and .89, respectively, if ensemble 1 is omitted.

Contrary to the time scale the Lagrangian length scale remains nearly constant for the meridional component (dots in Fig. 6b), whereas the zonal one shows a similar behavior as the time scale. The arrows in Figure 6b denote ensembles 1 and 2, which are separated by the Azores front. This figure again shows the marked difference in zonal scales north and south of that front.

The anisotropy in the time scale requires more energy at the low frequency end of the spectra of the zonal component u' than v' (see also discussion under 6c). As the energy in this spectral range is low compared to the energy in the eddy band, this anisotropy does not show up in the r.m.s. velocities.

One possible interpretation of Figure 6 is as follows:

— the r.m.s. velocities north of the Azores are dominated by eddies and meanders. From satellite images we know that the meridional excursions of the meanders are of similar scale as the eddy size. The zonal wave length of the meanders, however, is larger than the eddy size.

— the meridional length scale characterizes both the eddy scale and the scale of the meanders. With respect to meridional displacements a particle cannot distinguish between eddies and meanders. It remembers a path of about 45 km.

— the zonal length scale is different for eddies and meanders. Additionally, the r.m.s. velocity in zonal direction is smaller in meanders than in eddies, thus, with increasing velocity $\sqrt{\overline{u'^2}}$ eddies dominate the dynamics with the same length scale for $\sqrt{\overline{u'^2}}$ and $\sqrt{\overline{v'^2}}$ whereas for small $\sqrt{\overline{u'^2}}$ meanders are becoming increasingly important with longer length scales.

— the behavior of the integral time scale is the direct consequence of this interpretation. Where eddies are dominating (high velocities) a particle has a short memory (2–4 days) because it has to change direction soon. The meridional time scale increases with decreasing velocity because a particle stays longer on a "straight" path if it moves slower. The zonal time scale increases faster with decreasing velocity because particles in meanders stay longer on a "straight" path due to longer scales in zonal direction.

Ensemble 1 south of the Azores front fits into this interpretation: whereas in the area north of the Azores slow r.m.s. velocities are indicative of the dominance of meanders, these meanders are missing in the subtropical gyre. There in the eastern recirculation area, the eddies are weak and are of similar size as elsewhere. Therefore, we find the typical eddy length scale south of the Azores front associated with low velocities and a

time scale corresponding to that. This is further supported by the spectra in Figure 15. Ensemble 1 contains the lowest energy at low frequencies compared to all other spectra.

Finally, it may be instructive to derive an eddy scale, as a particle sees it. If the length scale, over which the particle remembers its path, is of the order of 50 km and if we consider the path in a circular eddy as straight during a 45° sector of this circle, a typical eddy diameter is $8L/\pi$, which corresponds to about 130 km.

6. Single particle dispersion

We next test Taylor's theorem for the two cases $t < T$ and $t > T$. As outlined by Colin de Verdiere (1983) the data base for the statistical description of diffusion can be considerably increased by making use of homogeneity and stationarity. The time series of daily positions were split up into a number of time series starting after a multiple of 10 days which is generally larger than the decorrelation time of the drifters. The method breaks down if the assumptions of homogeneity and stationarity are validated, but the same holds for the relation derived from the Taylor theorem, which we are going to test.

In Figure 7 we display the dispersion in x- and y-direction as function of time for the entire range up to 160 days. Ensembles 2 and 5 at mid-latitudes serve as examples. Similar to the calculation of the autocorrelation function or the structure function we encounter the problem that with increasing time the number of data points becomes smaller and random fluctuations may become dominant. Bearing this in mind, we may distinguish three regimes:

(i) a rapid increase in dispersion during the initial time after release.

(ii) a reduced increase between about 10 and 60 days.

(iii) a tendency for a saturation level after about 80 days which gives an upper bound to horizontal dispersion.

a. The initial dispersion. According to (8) the initial dispersion should increase with t^2 according to Taylor's result. Freeland *et al.* (1975) concluded from their floats in 1500 m depth that homogeneous turbulence was not capable of describing the dispersion in the MODE region. Their main argument was that the computed slopes of the dispersion curves were less than expected. Colin de Verdere (1983) on the other hand found excellent agreement between predicted and computed initial dispersion. However, after a few days, the rate of increase of the dispersion was less than the variance, and after 10 days the random walk regime was reached.

Our results show the same general behavior. Taylor's initial dispersion should hold in the limit $t \to 0$. As shown in Figure 8—with the exception of the meridional dispersion in the less reliable ensemble 8—predicted and computed dispersions are in

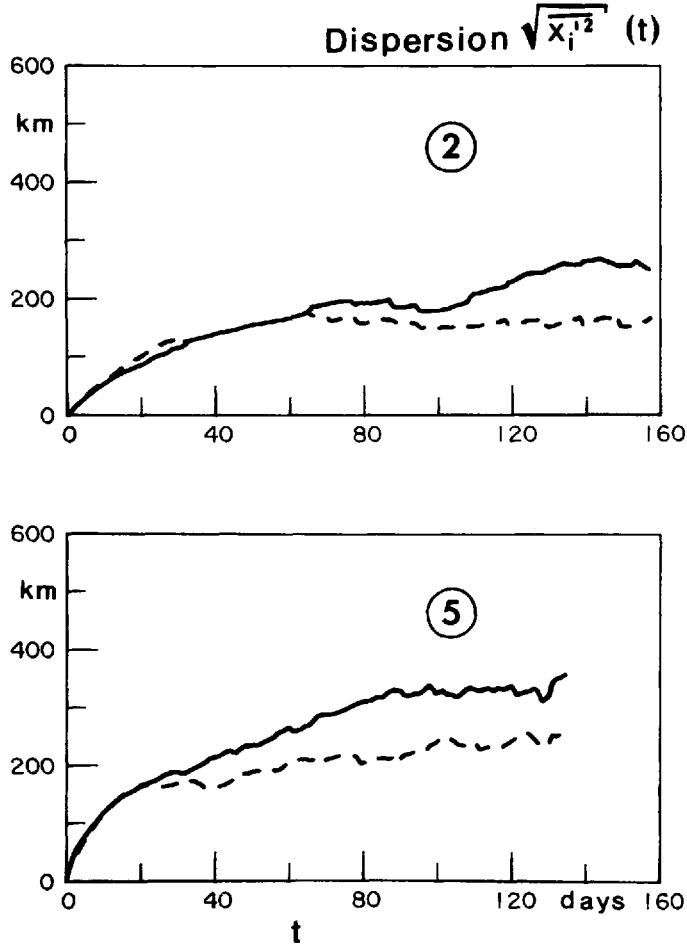

Figure 7. Single particle dispersion for ensembles 3 and 5. (Full line zonal, broken line meridional dispersion.)

excellent agreement during the first, sometimes even during the second day. After that time dispersion increases slower, but still according to our expectation. The transition range between the initial range and the random walk regime depends—according to (7)—on the autocorrelation function. In order to interpret the deviation of the observed curves from the theoretical ones in Figure 8 we use the ideal case, $R(\tau) = \exp(-\alpha\tau^2)$. In Figure 9 we display hypothetical dispersion curves computed from (7) with α ranging from 0.01 to 0.1. The corresponding Lagrangian time scales are 8.86, 3.96 and 2.80 days respectively and $\sqrt{\overline{u'^2}} = 11.5$ cm s^{-1}. The shorter the integral time scale, the shorter is the initial range and the slower increases dispersion after about two days. Thus, with Lagrangian integral time scales as given in Table 3 (upper bounds) or 4, we

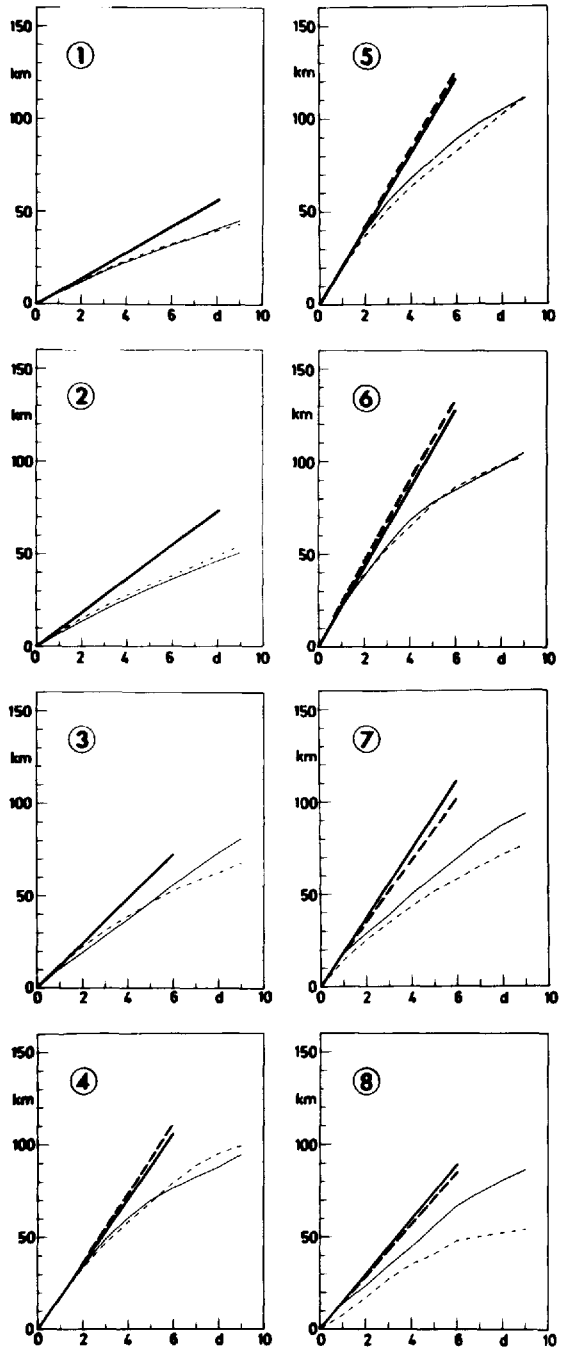

Figure 8. Single particle dispersion during the initial phase dispersion in km, time in days. Full and broken heavy lines refer to Eq. (8), thin lines are observations. Full lines are zonal, broken ones are meridional dispersions.

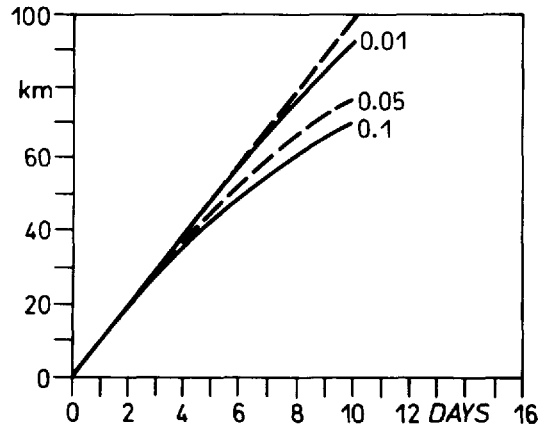

Figure 9. Single particle dispersion for the ideal case $R(\tau) = e^{-\alpha\tau^2}$, α = 0.01, .05 and .1, respectively.

cannot expect the initial phase to extend over more than 1–2 days. During the first day, however, the coincidence is nearly perfect. We further note that according to Table 3 the meridional time scales are shorter in most ensembles and consequently, the meridional dispersions in Figure 8 increase slower than zonal dispersion.

b. The random walk regime. After about 10 days particles are dispersed by about 50-100 km from their origin according to Figure 8. In Figure 10 we depict both ranges in a log-log-scale, the initial and the random walk regime. Heavy lines indicate the power laws for both ranges. As during the initial phase the curves show good agreement with theory if the random walk regime is defined as the range from about 10–60 days.

Another feature may be noticed: as seen from Figure 8 dispersion is isotropic during the first day. With increasing time, however, there is a tendency for the meridional dispersion to become smaller than the zonal one. This holds at least for the northernmost ensembles, Nos. 3, 5, 6, 7, and 8.

If this were due to the β-effect (Haidvogel, 1984) one would expect to see the anisotropy more pronounced in the low intensity eddy field at lower latitudes, where the relative influence of β is larger. We interpret the deviation as being due to the shear of the mean field.

According to Table 2 the mean zonal velocity increases from 0 to 8 cm s^{-1} between 30N and 50N. Typical standard excursions of the particles are $\pm 2°$ meridionally according to Table 1, which may include individual excursions much larger. In the Appendix we show the effect of the shear of the mean field on autocorrelation function and dispersion. The higher dispersion in zonal direction may well be due to the fact that the mean field is not sufficiently constant over the latitude belt in the northern part of

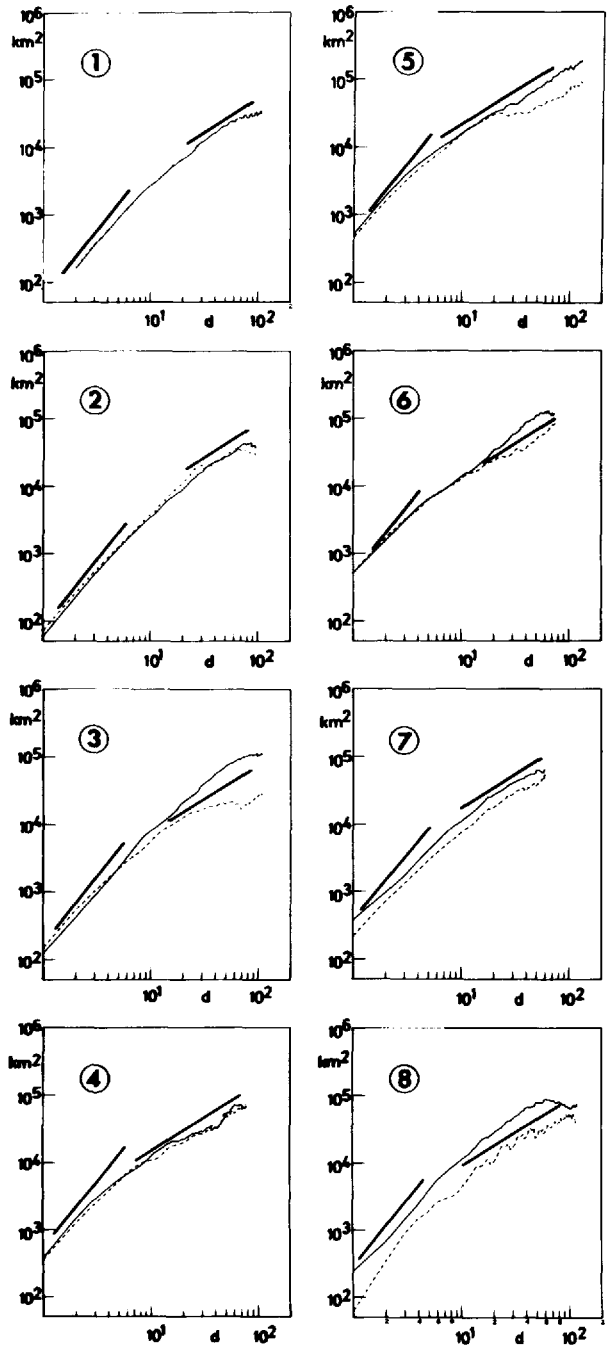

Figure 10. Single particle dispersion between 1 and about 100 days in a log-log plot. Heavy line gives power law according to Eqs. (8) and (9). Otherwise like Figure 8.

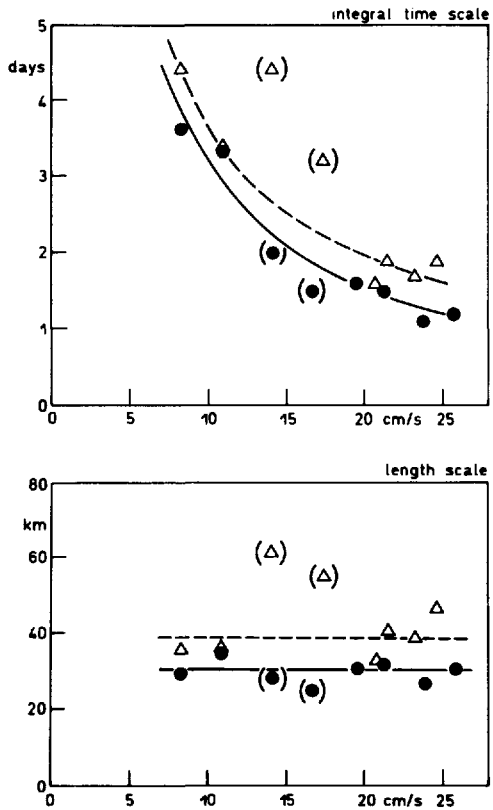

Figure 11. Integral time scale and length scale as function of r.m.s. velocity derived from dispersion. Otherwise like Figure 6.

the North Atlantic, over which the particles disperse. Thus part of the shear of the mean field may be interpreted as dispersion.

The dependency of the dispersion on the integral time scale in the random walk regime may be used for an independent calculation of T. The results are listed in Table 4 and are plotted in Figure 11. The values for T and L are shorter than those given in Table 3 where upper bounds for T had been derived. Regression analysis confirms the inverse proportionality between T and $\sqrt{\overline{u'^2}}$:

$$T_{11} = 0.28 + 33.6/\sqrt{\overline{u'^2}} \qquad T_{22} = -0.04 + 31.8/\sqrt{\overline{v'^2}}. \tag{13}$$

In both cases correlation coefficients of 0.99 are obtained, if ensembles 3 and 8 are omitted.

Contrary to Figure 6 also the zonal length scale is constant, if ensembles 3 and 8 are considered to be not reliable. The mean values are $L_{11} = 39$ km, $L_{22} = 31$ km. Consistent with the interpretation given in the previous section 5, we believe that the

results shown in Figure 11 are more reliable than those in Figure 6. If meanders contribute in the low velocity range, the autocorrelation function should have negative lobes. Consequently, the integral time scale given by the first zero crossing is too large, and so is the length scale.

c. The saturation level. According to Figure 7 dispersion tends to get saturated after about 60–80 days which sets an upper-bound for the random walk regime. Maximum displacements reached by the particles are about 200–300 km, again yielding larger values for the zonal displacement.

We consider the saturation level in Figure 7 to be the result of two factors. Both may best be discussed in the spectral domain. According to Eq. (7) the displacement can be obtained for any time t by integrating the Lagrangian spectrum multiplied by the sinc-weighting function,

$$\overline{x'^2}(t) = 2t \int_0^\infty E\left(\frac{2q}{t}\right) \frac{\sin^2 q}{q^2}\, dq,\ q = \frac{\omega t}{2}. \tag{14}$$

The sinc-function implies that only the range $0 < q < \pi$ contributes to the integral, which vice versa requires energy in the spectral range $0 < \omega < 2\pi/t$. Likewise, if we use frequencies f instead of circular frequencies, we require the spectrum E in the range $0 < ft < 1$. For dispersion times t of 100 days, e.g. the spectrum is needed for frequencies $f < 3.10^{-4}$ cph, which is only partially available from the present data set. The spectra in Section 8 show that the energy level is rather low at low frequencies. We therefore conclude that both the limited time series of 5 months and the low energy content at the shorter end of the spectral range contribute to limit the dispersion.

7. Eddy diffusivity

Eddy diffusivities can be calculated according to any of the definitions given by Eq. (10). In Figure 12 we display diffusivities in zonal (K_{11}) and meridional (K_{22}) direction according to $(d\overline{x'^2}/dt)/2$ for ensemble 1. As $\overline{x'^2}$ increases linearly with time in the random walk regime, eddy diffusivity should reach a constant plateau after about 10 days. This plateau is recognized in Figure 12 for the range from day 10 to day 40, approximately. Due to differentiation small deviations from linearity appear as rather large oscillations. After about 40 days the data set becomes too small and random variations become dominant. Nevertheless, the mean value of the plateau between 10 and 40 days establishes the value of the eddy diffusivity.

Instead of differentiating $\overline{x'^2}$ we use the last relation in Eq. (10) to compute eddy diffusivities for all 8 ensembles. They are listed in Table 4, columns 4 and 5, and are based on the Lagrangian time scale according to columns 2 and 3 in Table 4. Eddy diffusivities increase from southeast (ensemble 1) toward the Subarctic front approximately by a factor of 4 and become strongly anisotropic north of 45N. In Figure 13 we

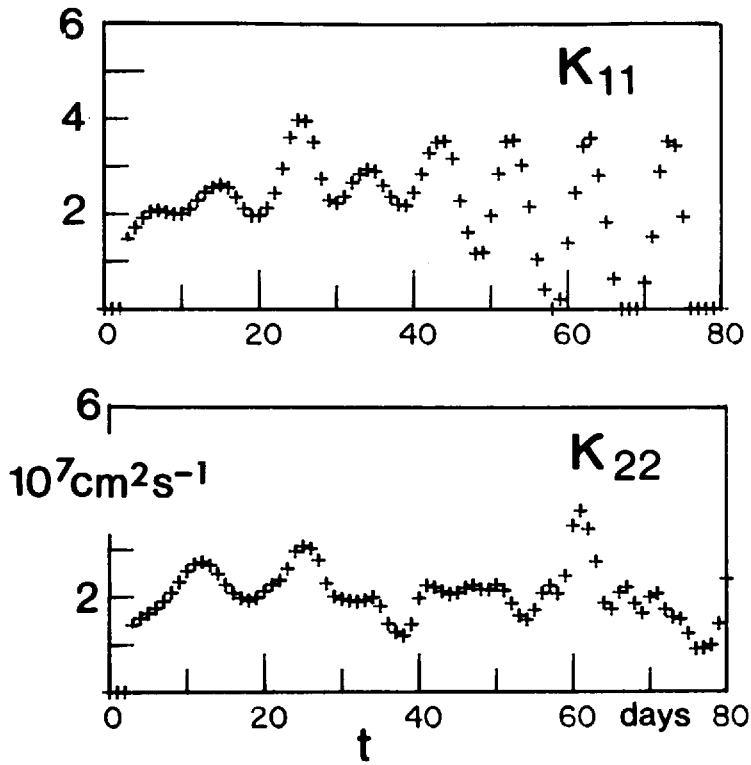

Figure 12. Zonal (K_{11}) and meridional (K_{22}) eddy diffusivities according to $K_{ii} = (d\overline{x_i^2}/dt)/2$.

Table 4. Lagrangian time scales, eddy diffusivity, and Lagrangian length scale as derived from single particle dispersion.

	Time scale (d)		Eddy diffusivity (10^7 cm^2 s^{-1})		Length scale (km)	
Ensemble	zonal	meridional	zonal	meridional	zonal	meridional
1	4.4	3.6	2.5	2.1	36	30
2	3.4	3.3	3.5	3.3	37	35
3	4.4*	2.0	7.5*	3.5	62*	28
4	1.6	1.5	5.8	5.8	33	32
5	1.7	1.1	8.1	5.2	39	26
6	1.9	1.2	9.8	6.9	47	31
7	1.9	1.6	7.5	5.2	41	31
8	3.2**	1.5**	8.4**	3.6**	55**	25**
Mean	2.8	2.1	6.6	4.5	39	31

*t^1-Regime is not well-defined
**Only 4 drifters

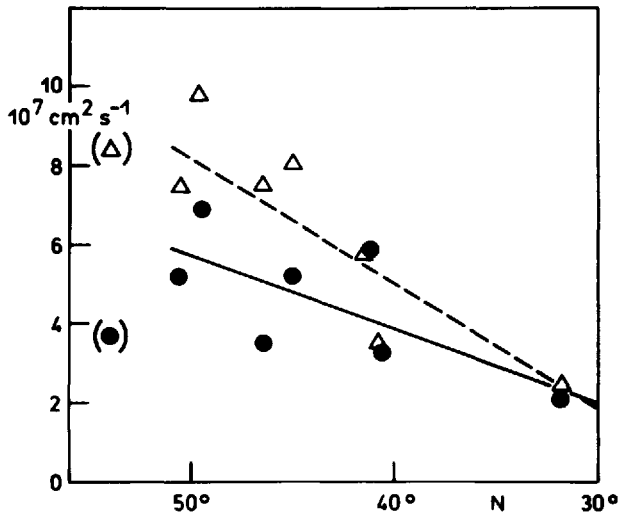

Figure 13. Eddy diffusivity between 30N and 50N. Triangles are zonal, dots are meridional diffusivities.

depict K as function of latitude, which demonstrates the increase in K with increasing latitude. Between 30N and 50N zonally averaged eddy diffusivities at 100 m depth are given by

$$K_{11}(\phi) = (-9.4 + 0.36\phi)\ 10^7\ \text{cm}^2\,\text{s}^{-1}$$
$$K_{22}(\phi) = (-3.6 + 0.19\phi)\ 10^7\ \text{cm}^2\,\text{s}^{-1} \qquad (15)$$

where ϕ is latitude in degree. The correlation coefficients for these regression lines are 0.89 and 0.72, respectively. As variable eddy diffusivity implies a transport of scalar quantities, we expect a southward eddy transport in the North Atlantic between 30N and 50N. Roughly speaking, the eddies induce a meridional Lagrangian mean advection speed of $v = -dK_{22}/dy = -0.18$ cm s^{-1}, which has to be compared with $\bar{v}$ in Table 2.

Besides the meridional dependency of the eddy viscosity we are also able to relate K to the r.m.s. velocity of the eddy field. Rossby *et al.* (1983) related diffusivity in the western North Atlantic, at a variety of depths, linearly to the local eddy kinetic energy. This implies the integral time scale to be constant, which clearly does not hold according to our results. Furthermore, using floats from different levels between 700 m and 2000 m for the derivation of a relationship implies that the variables related to each other must be depth independent. Otherwise the relation may be biased by the depth structure (Böning and Cox, 1987).

Our results are depicted in Figure 14. They cover a wide range of r.m.s. velocities

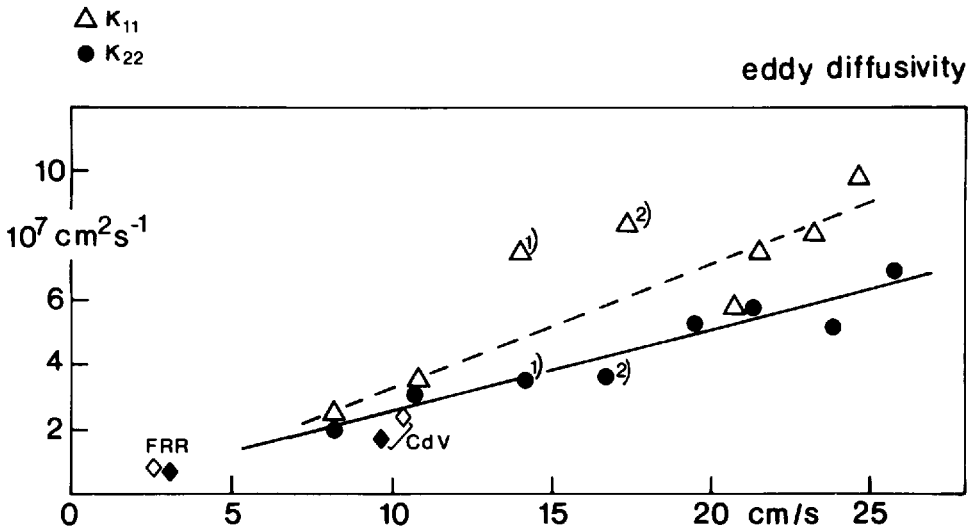

Figure 14. Eddy diffusivity as function of r.m.s. velocity. Triangle and dots as in Figure 13. (FRR = Freeland *et al.*, 1975, CdV = Colin de Verdiere, 1983).

and show a clear linear relation between eddy diffusivity and r.m.s. velocity. The values of Colin de Verdiere (1983) are included in the figure and so are those of Freeland *et al.* (1975), labeled as CdV and FRR, respectively. Our points (1) and (2) belong to ensembles 3 and 8, respectively. In ensemble 3 the random walk regime (Fig. 10) is not very well established, ensemble 8 consists of only 4 buoys. If these two groups are excluded we obtain a rather strong linear relation between eddy diffusivity and r.m.s. velocity at 100 m. These relations are

$$K_{11} = (-0.9 + 0.39\sqrt{\overline{u'^2}})\ 10^7\ \text{cm}^2\,\text{s}^{-1}$$
$$K_{22} = (0.5 + 0.23\sqrt{\overline{v'^2}})\ 10^7\ \text{cm}^2\,\text{s}^{-1} \qquad (16)$$

for the range from 5 to 30 cm s^{-1}. In both cases the correlation coefficient is 0.96. The simple relation $K = L\sqrt{\overline{u'^2}}$ states a direct proportionality between eddy diffusivity and eddy r.m.s. velocity, the proportionally constant being an effective mixing length. The value of this length is 39 km in zonal and 31 km in meridional direction.

A linear relationship between diffusivity and eddy velocity can be expected on dimensional grounds, if the diffusivity depends on eddies of nearly constant size and the eddy velocity. It has been anticipated e.g. by Armi (1979) and McWilliams *et al.* (1983) and was also obtained in numerical models (Haidvogel and Keffer, 1984).

The impact of the above results on mixing of scalar quantities by eddies is further explored in Section 9. We first conclude the statistics by describing the Lagrangian spectra.

8. Lagrangian energy spectra

Estimates of the Lagrangian spectra presented in Figures 15a–15c were obtained by dividing each drifter time series into 128-day pieces, computing the spectra for each piece and averaging over the available number of pieces. These range between 10 and 25. A Hanning window has been applied. Results are displayed for ensembles 1, 2, 4, 5, 6, and 7. Ensembles 3 (badly developed random walk regime) and 8 (only 4 buoys) have been omitted. Each spectrum is shown in an energy conserving and in a log-log plot. The energy conserving spectra show a systematic shift of the eddy energy containing band. At low latitudes (ensembles 1 and 2) eddy energy is concentrated between about 20 and 50 days whereas further to the north the eddy containing range shifts to 5–20 days. Further note the change in scale between Figures 15a, b, and c. In ensembles 1 and 2 eddy energy reaches values of about 40 $cm^2 s^{-2}$, in ensembles 6 and 7, however, maxima of more than 500 $cm^2 s^{-2}$ are obtained. This result is consistent with the Lagrangian time scales derived above: eddies are of approximately equal size in the North Atlantic between 30N and 50N but energy increases in these eddies with increasing latitude. Consequently, a particle needs less time to surround a strong eddy, yielding shorter time scales in the north.

In the log-log-plot the spectra consist of a low-frequency plateau which extends up to the cut-off frequency given by the frequency of the energy containing eddies. This frequency is marked by an arrow in each spectrum and the corresponding time scale (days) is given. Beyond the cut-off frequency the energy drops rapidly. It is difficult to design a distinct slope to the spectra. Freeland *et al.* (1975) obtained slopes like -4 in 1500 m depth, Colin de Verdiere (1983) obtained a well defined -2 slope within a 4–10 day band. Our spectra fall off predominantly according to -2, but there are cases (ensembles 4 and 5) which are better described by a slope of -3.

Compared to Eulerian spectra (Dickson, 1983) Lagrangian spectra reveal similar characteristics: there exists an increase of eddy kinetic energy with increasing latitude and a corresponding reduction in period of the most intensive energy band. Furthermore, a dominance of a -2 slope is also observed in Eulerian spectra (Colin de Verdiere, 1983). However, the relationship between Eulerian and Lagrangian spectra is complicated. The Lagrangian frequency spectrum may be regarded as a broadened version of the Eulerian energy spectrum. According to Middleton (1985) this feature is associated with the result that the Lagrangian time scale is shorter than the Eulerian time scale. Simply speaking, a particle encounters an eddy faster than the eddy moves across a mooring site. The similarity in spectral slope results from the slope correspondence between the Lagrangian frequency and the Eulerian wave number spectra. The broadening is then determined by the Eulerian advective velocity time scale.

9. Discussion

From studies with eddy resolving models it is clear that the eddy field can strongly modify the mean circulation of the ocean. Eddy kinetic energy in most regions of the

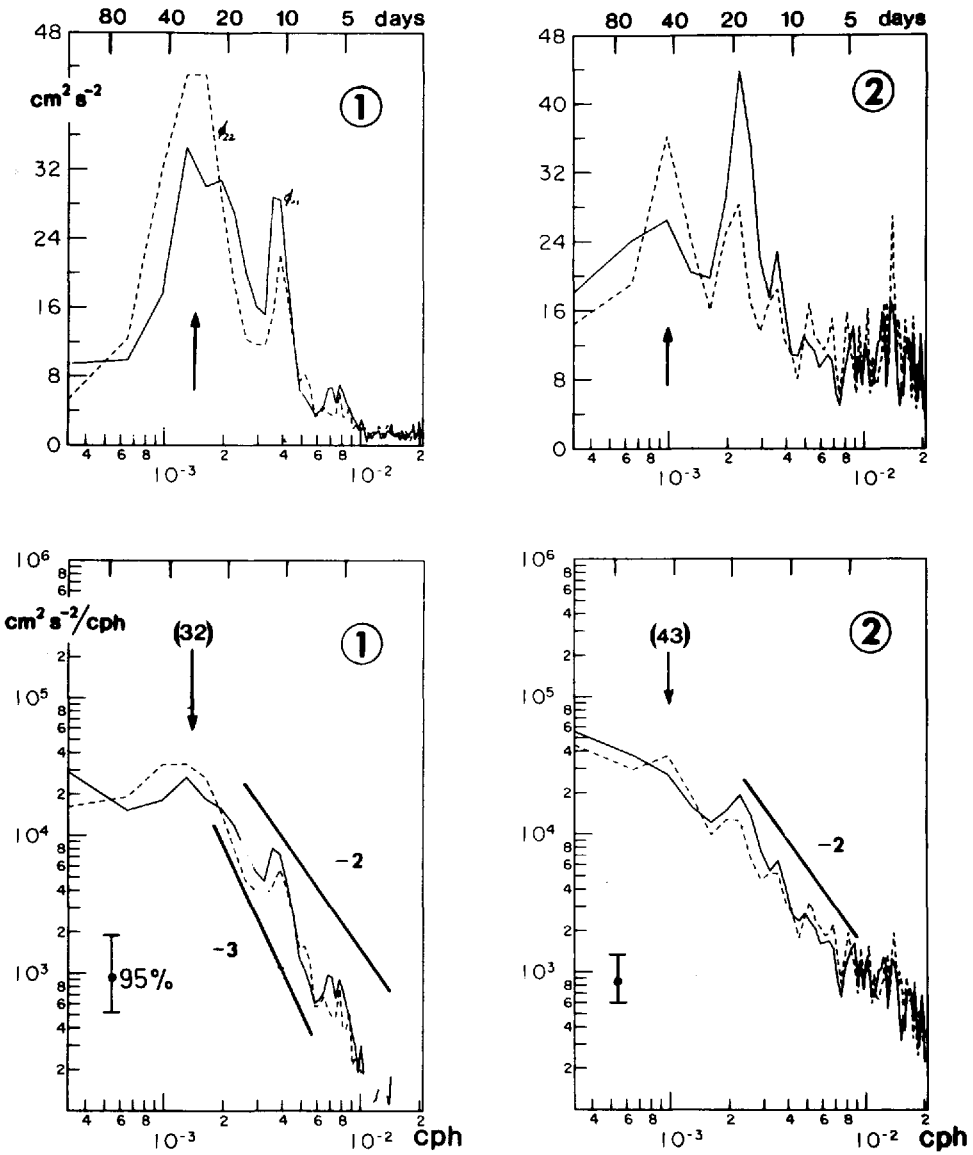

Figure 15a. Lagrangian spectra in an energy conserving (top) and log-log-plot for ensembles 1 and 2. Arrow and number marks cut-off frequency and corresponding time in days.

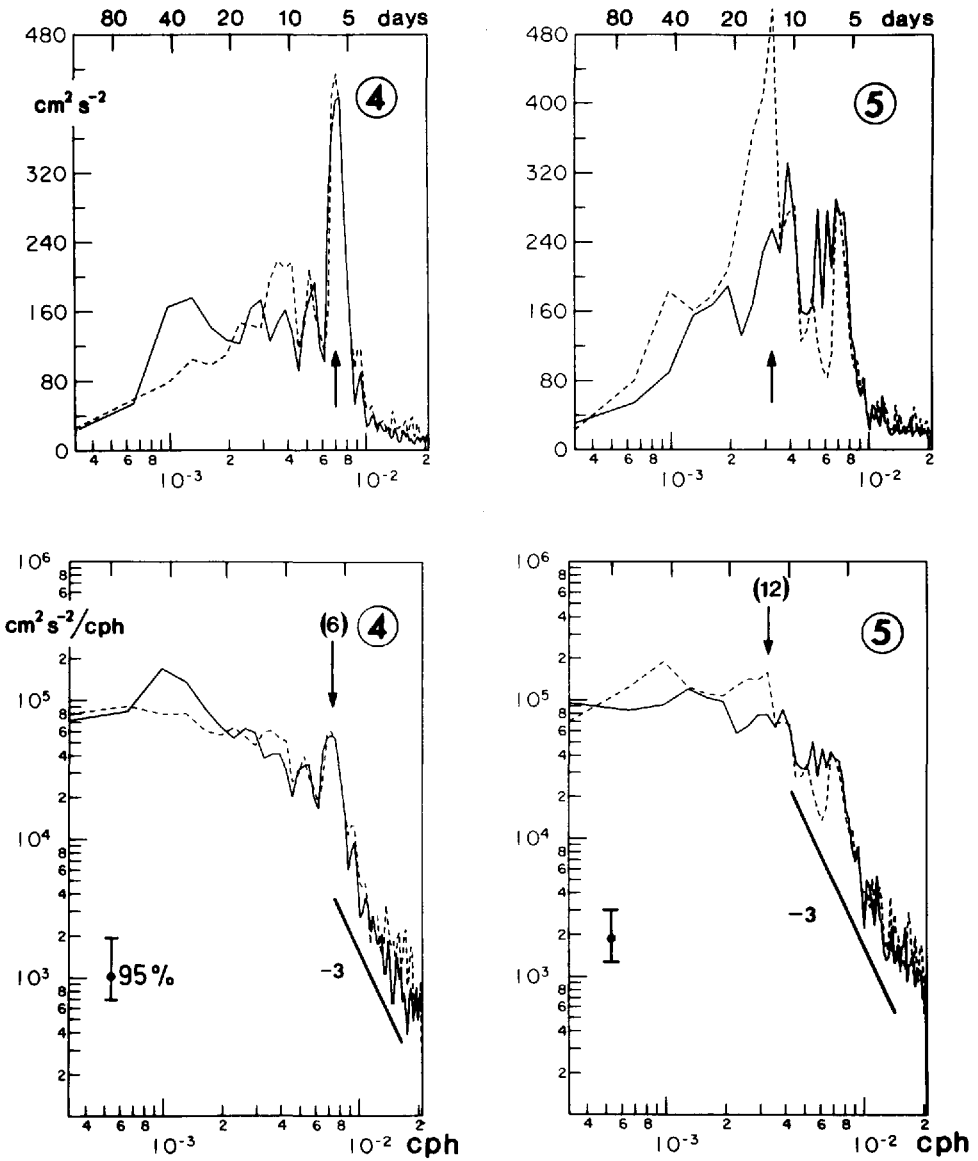

Figure 15b. Same as Figure 15a for ensembles 4 and 5.

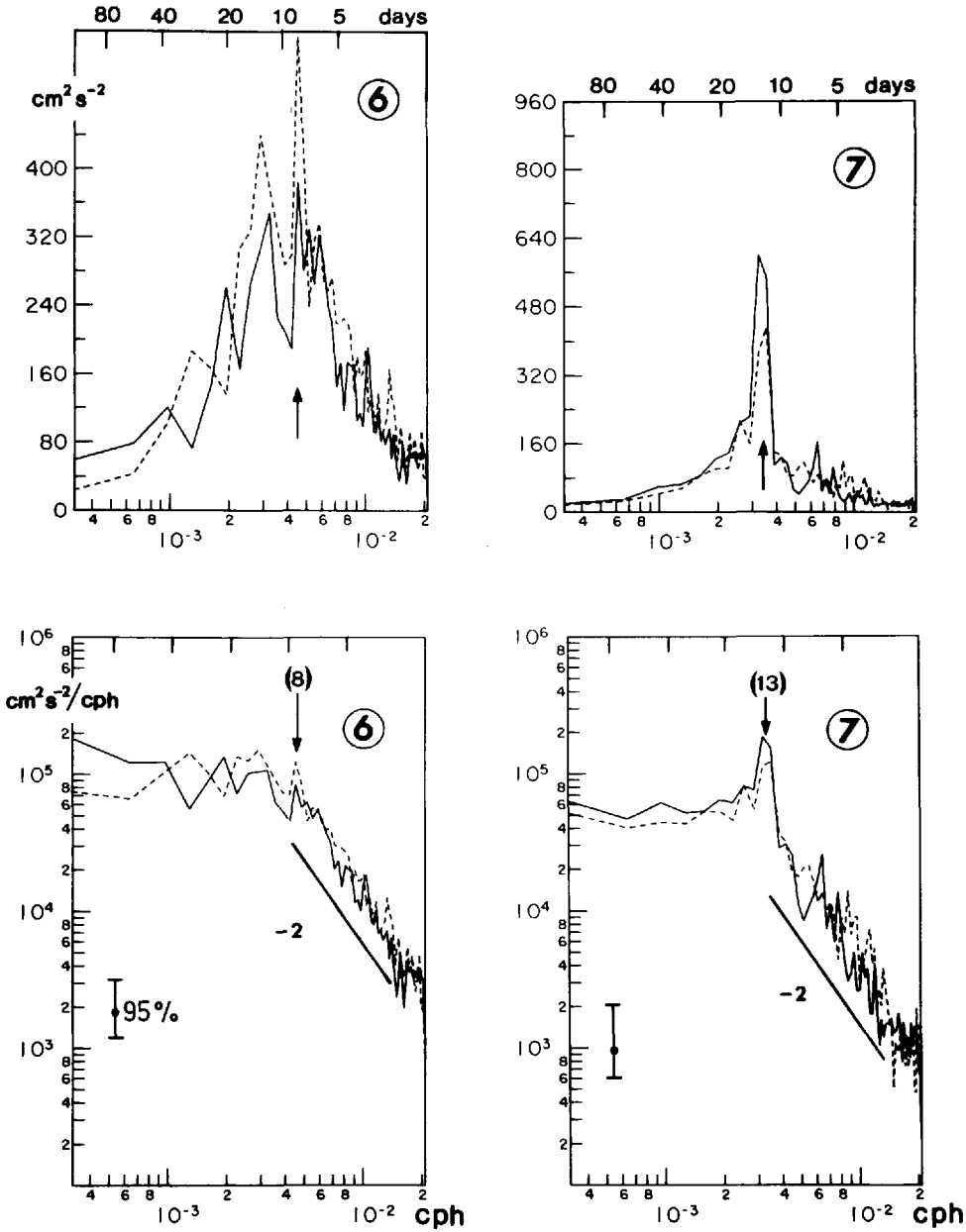

Figure 15c. Same as Figure 15a for ensembles 6 and 7.

North Atlantic Ocean is several times larger than the mean value and an instantaneous glimpse of the flow is nearly always dominated by the eddy field.

Eddy resolving models have largely enhanced our knowledge on ocean dynamics, however, the large number of experiments with these eddy resolving models also establish that there is considerable model sensitivity to changes in the model physics. Thus, among others, a better understanding of the mixing processes is required.

On the other hand, the traditional assumption in coarse resolution studies to relate the effects of the mesoscale eddy field to a constant diffusivity times the Lagrangian of the mean field, is a very poor approximation. The eddy fields are considerably more complex spacially than are the fields of the Lagrangians of the mean fields, therefore, no satisfactory correlations (Harrison, 1978) between these fields may be found unless a detailed knowledge of the diffusivity is available. A recent experiment on passive tracer transport carried out with an eddy-resolving model and compared to a parallel computation with greater viscosity and diffusion, which supressed the mesoscale eddies, showed large differences between both distributions. A sharpe tongue of tracer from the outcrop region is formed on the equatorward flank of the subtropical gyre in the noneddy resolving case, when eddies are included, this tongue becomes blurred. Isopycnal mixing is considerably increased in case of very high resolution (Cox, 1985).

Passive tracers, subsurface floats and satellite-tracked buoys can be used for a better understanding of large-scale oceanic mixing and for developing better parameterization of eddies in models of the general circulation. The present data set is especially qualified for studies of this type, because quite a number of buoys have been deployed in rather limited areas during hydrographic surveys, which were aimed to monitor the eddy field. The results obtained cover a large area of the North Atlantic from which no information on Lagrangian statistics was available previously. They are summarized in Figure 16 with respect to eddy kinetic energy and diffusivity.

Eddy kinetic energy increases from about 70 $cm^2\ s^{-2}$ in the eastern basin to more than 600 $cm^2\ s^{-2}$ in the North Atlantic Current at the Subarctic Front and in the eddy field of the Gulfstream extension area east of Flemish Cap. It is isotropic in all areas. The Lagrangian time scale, however, is anisotropic being larger in zonal than in meridional direction, which is already evident from inspection of the autocorrelation functions R_{11} and R_{22}. This has been anticipated by Rhines (1976) and has been further elucidated by Haidvogel (1984). Using a barotropic eddy resolving model, Haidvogel studied the dispersion of particles in a homogeneous turbulent flow on a β-plane, spanning the parameter range from pure two-dimensional turbulence to a strongly wave-like flow field. He showed that Taylor's Theorem holds only for very weak β. With increasing β-effect, single particle dispersion is greatly enhanced in zonal direction and suppressed in meridional direction.

As mentioned above determination of Lagrangian time scales from real data requires a large set of drifters, which is barely available at present. However, the

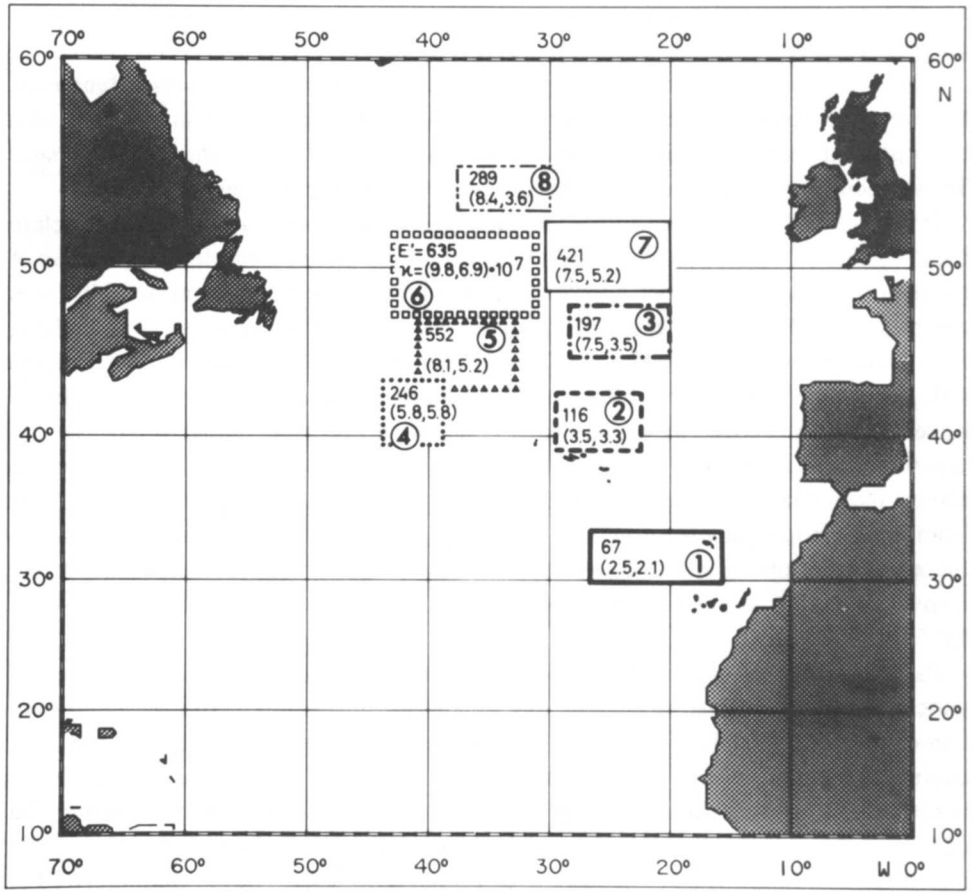

Figure 16. Eddy kinetic energy E' and eddy diffusivity (K_{11}, K_{22}) in the North Atlantic.

systematic difference between T_{11} and T_{22} in most areas of this study indicate that the anisotropy of these values is well established. Furthermore, the high confidence of the isotropy of the r.m.s. velocities justifies the conclusion that the same anisotropy holds for the Lagrangian length scale and the diffusivity. Whether this is a consequence of the β-effect may remain an open question.

Due to the increase of the velocity variance from southeast toward northwest in the North Atlantic, diffusivity shows a similar increase besides the reduction of the time scale. This has been suggested already from a preliminary study (Krauss and Käse, 1984). The values obtained are in the range of earlier studies on the eastern and western side of the North Atlantic. Colin de Verdiere (1983) obtained $K_{11} \simeq K_{22} \simeq 2 \cdot 10^7$ cm^2 s^{-1} in the Biscaye, McWilliams *et al.* (1983) reported $(K_{11}, K_{22}) = (8 \cdot 10^7, 5 \cdot 10^7)$cm^2 s^{-1} in the LDE area in 700 m depth. Riser and Rossby (1983) obtained $(K_{11}, K_{22}) = (4.5 \cdot 10^7, 1.8 \cdot 10^7)$ cm^2 s^{-1} from float data at 700 m depth in the

area between 10N–26N and 70W–50W whereas Freeland *et al.* (1975) arrived at $(K_{11}, K_{22}) = (0.78 \cdot 10^7, 0.71 \cdot 10^7)$ cm^2 s^{-1} in the MODE area, which is known as being very calm. Our values increase from $(K_{11}, K_{22}) = (2.5 \cdot 10^7, 2.1 \cdot 10^7)$cm^2 s^{-1} in the Canary Basin to $(K_{11}, K_{22}) = (9.8 \cdot 10^7, 6.9 \cdot 10^7)$ cm^2 s^{-1} in the Newfoundland Basin, where very vigorous eddy fields are observed.

Thus there seems to evolve a consistent picture of slightly anisotropic Lagrangian diffusivity which changes by a factor of 4 from the eastern and southeastern North Atlantic (30N) to the Gulf Stream extension area and the North Atlantic Current (50N).

The ability of eddies to transport dynamically passive tracers has important consequences for the distribution of these properties in the ocean. Knowing diffusivity due to eddy fields quantitatively in a much greater detail as is presently the case would yield a powerful parameterization of mesoscale eddy mixing. Simple advective-diffusive models of tracer dispersal, in which eddy effects are parameterized as anisotropic diffusivity functions of space, would allow a better understanding of the observed distributions (Armi and Haidvogel, 1982). To a first approximation this holds also for nonpassive quantities like heat and salt flux by mesoscale eddies.

Acknowledgments. We acknowledge the support of the German National Science Foundation (SFB 133).

APPENDIX

Influence of current shear on the statistics

In computing quantities from drifters we assumed a constant mean value $\bar{u}$ for the area under consideration. If this is violated the following errors are induced:

Suppose a meridional shear in the mean zonal velocity,

$$u = \bar{u}(y) + u', \qquad \bar{u}(y) = u_0 + u_1 y. \tag{1}$$

Instead of the real mean $\bar{u}(y)$, we use

$$\bar{\bar{u}} = \frac{1}{B}\int_0^B u(y)dy = u_0 + u_1 B/2. \tag{2}$$

Therefore, our statistics are computed for u'', where

$$u = \bar{\bar{u}} + u'', \qquad u'' = u' + u_1(y - B/2). \tag{3}$$

The autocorrelation function obtained for u'' is

$$R(\tau) = R_t(\tau) + \epsilon^2/u''^2, \qquad \epsilon = u_1(y - B/2) \tag{4}$$

where $R_t(\tau)$ is the true autocorrelation function due to u', i.e. the correlation function is parallel shifted to higher values and, therefore, may not approach zero. The Taylor

theorem takes the form

$$\overline{x''^2} = \overline{2u'^2} \int_0^t \left(\frac{\epsilon^2}{t} - \tau \right) R_t(\tau) + \epsilon^2 t^2 + 0\,(\overline{u'^2})^2 \tag{5}$$

for small t, $\overline{x'^2} = (\overline{u'^2} + \epsilon^2)t^2$ for $t \gg T$, $\overline{x'^2} = \overline{2u'^2}Tt + \epsilon^2 t^2$. Thus, a mean shear increases the computed zonal dispersion.

REFERENCES

Armi, L. 1979. Effects of variations in eddy diffusivity on property distributions in the oceans. J. Mar. Res., *37,* 512–530.

Armi, L. and D. B. Haidvogel. 1982. Effects of variable and anisotropic diffusivities in a steady-state diffusion model. J. Phys. Oceanogr., *12,* 785–794.

Böning, C. W. and M. D. Cox. 1987. Particle dispersion and mixing of conservative properties in an eddy resolving model. J. Phys. Res., (submitted).

Colin de Verdiere, A. 1983. Lagrangian eddy statistics from surface drifters in the eastern North Atlantic. J. Mar. Res., *41,* 375–398.

Cox, M. D. 1985. An eddy resolving numerical model of the ventilated thermocline. J. Phys. Oceanogr., *15,* 1312–1324.

Davis, R. E. 1983. Oceanic property transport, Lagrangian particle statistics, and their prediction. J. Mar. Res., *41,* 163–194.

—— 1985. Drifter observations of coastal surface currents during CODE: The statistical and dynamical views. J. Geophys. Res., *90,* 4756–4772.

Dickson, R. R. 1983. Global summaries and intercomparison: Flow statistics from long-term current meter moorings, *in* Eddies in Marine Science, A. R. Robinson, Ed., Springer Verlag, 278–353.

Flierl, G. R. and J. C. McWilliams. 1977. On the sampling requirements for measuring moments of eddy variability. J. Mar. Res., *35,* 797–820.

Freeland, H. J., P. Rhines and H. T. Rossby. 1975. Statistical observations of trajectories of neutrally buoyant floats in the North Atlantic. J. Mar. Res., *33,* 383–404.

Haidvogel, D. B. 1984. Particle dispersion and Lagrangian vorticity conservation in models of β-plane turbulence. (unpublished manuscript).

Haidvogel, D. B. and T. Keffer. 1984. Tracer dispersal by mid-ocean mesoscale eddies. Part 1: Ensemble statistics. Dyn. Atmos. Oceans, *8,* 1–40.

Harrison, D. E. 1978. On the diffusion parameterization of mesoscale eddy effects from a numerical ocean experiment. J. Phys. Oceanogr., *8,* 913–918.

Holland, W. R., D. E. Harrison and A. J. Semtner. 1983. Eddy-resolving numerical models of large-scale ocean circulation, *in* Eddies in Marine Science, A. R. Robinson, Ed., Springer Verlag, p. 329–403.

Kampé de Feriet. 1939. Le functions aleatoirs stationnaires et la theorie de la turbulence homogene. An. Soc. Sci., Bruxelles, *59,* 145–194.

Krauss, W. 1986. The North Atlantic Current. J. Geophys. Res., *91,* 5061–5074.

Krauss, W. and R. H. Käse. 1984. Mean circulation and eddy kinetic energy in the eastern North Atlantic. J. Geophys. Res., *89,* 3407–3415.

Krauss, W. and J. Meincke. 1982. Drift buoy trajectories in the North Atlantic Current. Nature, *296,* 737–740.

Levitus, S. 1982. Climatological atlas of the world ocean. NOAA Professional Paper, 13, 1–173.

McNally, G. J., W. C. Patzert, A. D. Kirwan, Jr. and A. C. Vastano. 1983. The near-surface circulation of the North Pacific using satellite tracked drifting buoys. J. Geophys. Res., *88,* 7507–7518.

McWilliams, J. C. *et al.* 1983. The local dynamics of eddies in the western North Atlantic, *in* Eddies in Marine Science, A. R. Robinson, Ed., Springer Verlag, 92–113.

Middleton, J. F. 1985. Drifter spectra and diffusivities. J. Mar. Res., *43,* 37–55.

Panchev, S. 1971. Random Functions and Turbulence. Pergamon Press, Oxford, 444 pp.

Rhines, P. 1976. The dynamics of unsteady currents, *in* The Sea, E. D. Goldberg *et al.*, eds., *6,* John Wiley, NY, 189–318.

Richardson, P. L. 1983. Eddy kinetic energy in the North Atlantic from surface drifters. J. Geophys. Res., *88,* 4355–4367.

Riser, S. C. 1982. The quasi-Lagrangian nature of SOFAR floats. Deep-Sea Res., *29,* 1587–1602.

Riser, S. C. and H. T. Rossby. 1983. Quasi-Lagrangian structure and variability of the subtropical western North Atlantic circulation. J. Mar. Res., *41,* 127–162.

Robinson, A. R. 1983. Overview and summary of eddy science, *in* Eddies in Marine Science, A. R. Robinson, Ed., Springer-Verlag, 3–15.

Rossby, H. T., S. C. Riser and A. G. Mariano. 1983. The western North Atlantic—A Lagrangian viewpoint, *in* Eddies in Marine Science, A. R. Robinson, ed., Springer Verlag, 66–91.

Schmitz, W. J., Jr. and W. R. Holland. 1982. A preliminary comparison of selected numerical eddy-resolving general circulation experiments with observations. J. Mar. Res., *40,* 75–117.

Taylor, G. T. 1921. Diffusion by continuous movement. Proc. London Math. Soc. Ser. A, *20,* 196–221.

Received: *25 June, 1986;* revised: *15 December, 1986.*